Dalton Transactions

Assessing structure and dynamics of iron complexes supported by tris(amidate)amine ligands

Journal:	*Dalton Transactions*
Manuscript ID	DT-ART-05-2025-001284
Article Type:	Paper
Date Submitted by the Author:	31-May-2025
Complete List of Authors:	Huffman, Lucy; University of Rochester, Chemistry Seshadri, Anjana; University of Rochester, Chemical Engineering Hastings, Christopher D.; University of Rochester, Chemistry Brennessel, William; University of Rochester, Department of Chemistry Franco, Ignacio; University of Rochester Barnett, Brandon; University of Rochester, Department of Chemistry

Assessing Structure and Dynamics of Iron Complexes Supported by Tris(amidate)amine Ligands

Lucy S. X. Huffman, Anjana Seshadri, Christopher D. Hastings, William W. Brennessel, Ignacio Franco, and Brandon R. Barnett*

Abstract: Chelating ligand platforms derived from tris(2-aminoethyl)amine (TREN) can facilitate low coordination numbers and provide opportunities to tune the steric and electronic profile of the secondary coordination sphere. Herein, we examine the ability of two related tris(amidate)amine ligands to stabilize low-coordinate complexes of trivalent iron, and further use molecular dynamics (MD) simulations to gain insight into the dynamics of both the primary and secondary coordination spheres. Our cavitand-inspired ligand allows for the isolation of four-coordinate **FeL^{OCH2O}** via oxidation of the anionic and isostructural ferrous precursor, demonstrating how the secondary sphere macrocycle can promote the retention of an open coordination site. Through comparison with a non-macrocyclized tris(amidate)amine ligand, molecular dynamics (MD) simulations are used to garner insights into how this macrocycle alters coordination sphere dynamics. Additionally, both four-coordinate **FeL^{OCH2O}** and five-coordinate **Fe(DMF)L^{OMe}** are shown to be synthons for the trigonal bipyramidal ferric fluoride complexes **[Fe(F)L^{OCH2O}]$^-$** and **[Fe(F)L^{OMe}]$^-$**, respectively.

Introduction

Synthetic coordination chemistry of iron is of broad interest owing to the metal's terrestrial abundance and privileged roles in enzymatic catalysis.[1–3] Many examples of high-valent iron containing metal-ligand multiple bonds are renowned for their abilities to activate strong bonds and functionalize organic substrates.[4–7] These reaction schemes frequently operate through trivalent intermediates, and compounds with the formal oxidation state of iron(III) often function

as synthetic points of entry into higher-valent systems.[8] These facts motivate the study of low-coordinate ferric compounds as both synthetic precursors and potential intermediates in bond functionalization reactivity.

Nature has evolved metalloenzymes bearing tailored microenvironments that guide productive and selective reactivity.[9] Synthetic ligand platforms seeking to emulate design principles common to biological scaffolds have explored the installation of various chemical motifs into the secondary coordination sphere, such as H-bond donors, H-bond acceptors, redox-inactive cations, and electrostatic charges.[10–14] In contrast, an often-overlooked structural aspect is the enforcement of empty space. For instance, protein tertiary structure often buries metallocofactor active sites within hydrophobic channels that promote substrate binding and protect the active site from the exterior environment.[15] However, promoting well-defined channels or pockets in small molecular complexes presents a challenge owing to the flexibility inherent to most molecular platforms in solution at ambient temperatures.

Recently, our group reported a cavitand-inspired tripodal ligand that orients a narrow macrocycle around a metal coordination site.[16,17] The small and rigid macrocycle profile can inhibit binding of small molecules to the metal on account of size. The trigonal monopyramidal ferrous compound $\mathbf{[FeL^{OCH2O}]^-}$ presents an open intracavity coordination site that can accommodate an axial ligand of appropriate size.[18] This species was shown to act as a synthon for the high-spin iron(IV)-oxo compound $\mathbf{[Fe(O)L^{OCH2O}]^-}$ which, on account of its extreme steric protection, exhibits remarkable kinetic persistence in solution.[18] Herein, we demonstrate that one-electron oxidation of $\mathbf{[FeL^{OCH2O}]^-}$ yields the neutral four-coordinate ferric compound $\mathbf{FeL^{OCH2O}}$, which we have structurally characterized. This species represents a very rare example of a trigonal monopyramidal ferric compound and, to our knowledge, the first to be characterized

crystallographically. The more flexible ferrous species **[FeL^{OMe}]$^{-}$** bearing a non-macrocyclized ligand can also undergo one-electron oxidation and be trapped through coordination of *N,N*-dimethylformamide (DMF) to yield the five-coordinate compound **Fe(DMF)L^{OMe}**. Both complexes are shown to be synthons for five-coordinate ferric species bearing an axial fluoride ligand. Additionally, molecular dynamics (MD) simulations have been used to interrogate the rigidity inherent to the [L^{OCH2O}]$^{3-}$ platform, and suggest a plausible route for intracavity ligand binding that avoids passage through the top of the organic macrocycle.

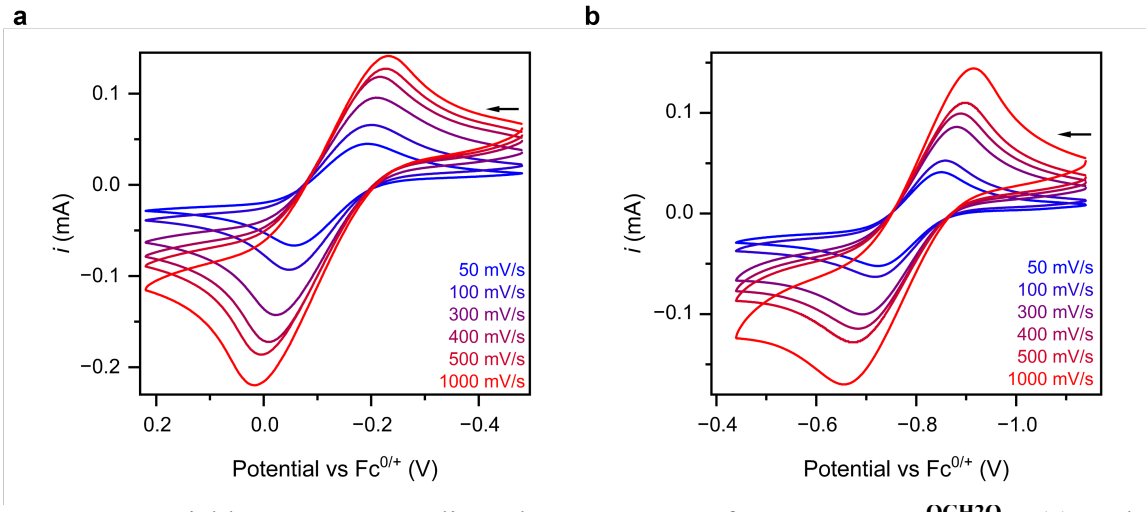

Figure 1. Variable scan rate cyclic voltammograms of 10 mM **[FeL^{OCH2O}]$^{-}$** (a) and 10 mM **[FeL^{OMe}]$^{-}$** (b) in DMF at 23 °C ([N(*n*-Bu)$_4$]PF$_6$ electrolyte).

Results and Discussion

While many trigonal monopyramidal complexes of iron(II) have been reported, isolable iron(III) species with this geometry are quite rare. Both Schrock and Casitas have reported the preparation of Fe^{III}(N(CH$_2$CH$_2$SiMe$_2$*t*Bu)$_3$),[19–21] although this complex has not been crystallographically characterized nor reported to be accessible in analytically pure form. Reports of other trigonal monopyramidal iron(III) complexes in TREN-derived coordination environments have not been accompanied by crystallographic characterization.[22,23] However,

coordination of exogenous or pendant donors has allowed for iron(III) species of higher coordination number to be prepared via chemical oxidation of their trigonal monopyramidal iron(II) counterparts.[24,25] Given the steric issues associated with ligand binding to $\mathbf{[FeL^{OCH2O}]^-}$ in particular, we decided to investigate the one-electron oxidation of both this species and its macrocycle-free congener $\mathbf{[FeL^{OMe}]^-}$, the synthesis of which is reported here for the first time (see ESI). Structural determination of $\mathbf{[FeL^{OMe}]^-}$ via single crystal X-ray diffraction reveals the expected coordination geometry of trigonal monopyramidal (Figure S33). From the solid state structure, a τ_4 parameter[26] of 0.85 is determined. This value is nearly identical to that displayed by $\mathbf{[FeL^{OCH2O}]^-}$ (τ_4 = 0.84),[18] in accord with the previous observation that the constrained macrocycle within $[L^{OCH2O}]^{3-}$ imparts only minor structural effects on the primary coordination within first-row metal complexes.[17]

As assayed through cyclic voltammetry in DMF, $\mathbf{[FeL^{OCH2O}]^-}$ and $\mathbf{[FeL^{OMe}]^-}$ display redox events at –0.13 V and –0.79 V vs. $Fc^{+/0}$, respectively, that are assigned to the $Fe^{III/II}$ redox couple (Figure 1a–b**)**. Given the electronically similar environments presented by the two tris(amidate)amine ligands,[16] the large difference in redox potentials suggests differing chemical speciation in solution. Both voltammograms show a pronounced dependence of the peak-to-peak separation on the scan rate, as well as a linear relationship between the square root of the scan rate and the peak current (Figures S1–2), indicating quasi-reversible electrochemical events.[27]

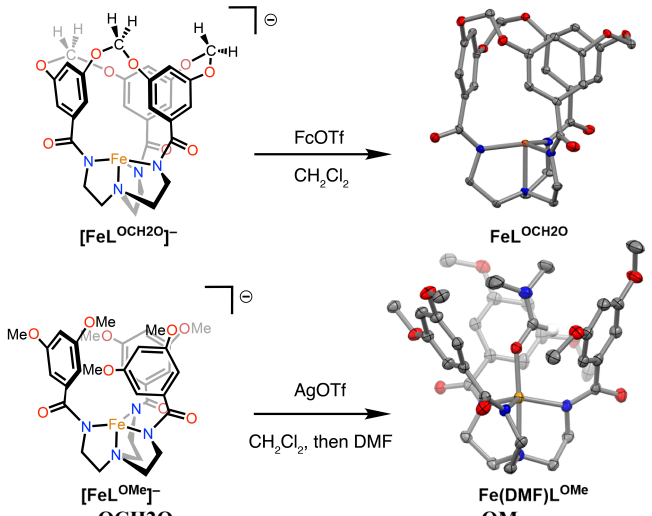

Figure 2. Syntheses of **FeL^{OCH2O}** (top) and **Fe(DMF)L^{OMe}** (bottom) with their solid-state structures. Hydrogen atoms and co-crystallized solvent molecules have been omitted for clarity. Thermal ellipsoids are shown the 50% probability level.

Chemical oxidation of **[FeL^{OCH2O}]$^{-}$** was performed using ferrocenium triflate (FcOTf) in CH_2Cl_2 (Figure 2). From the resulting brown residue, deep red crystals of the four-coordinate neutral species **FeL^{OCH2O}** that are suitable for X-ray diffraction can be isolated upon cooling to –35 ºC. This neutral complex is nearly isostructural with the anionic iron(II) congener (τ_4 = 0.84 for both complexes). The axial Fe–N_{amine} distance contracts by approximately 0.06 Å upon oxidation, the Fe–$N_{amidate}$ distances show contractions of a similar magnitude, and the iron center moves slightly closer to plane defined by the equatorial amidate nitrogens (Table S1). To our knowledge, **FeL^{OCH2O}** is the first structurally characterized ferric complex bearing a trigonal monopyramidal geometry.

While isolable in the solid state, **FeL^{OCH2O}** displays poor stability in solution (Figure S8), and the isolation of analytically pure samples has proven elusive. Red single crystals grown at –35 ºC are consistently contaminated with amorphous brown powders that are difficult to completely remove, while NMR analyses suggest the presence of remnant [K(Crypt)]OTf byproduct. Evans method measurements yield effective magnetic moments that are consistent

with the presence of paramagnetic iron-containing byproducts. Extended efforts to remove these impurities, or to access **FeL^{OCH2O}** using different oxidants, have not been successful. X-band EPR spectra of glassed solutions predominantly display one peak at g ≈ 4.3, corresponding to a rhombic S = 5/2 species (Figure S28). Indeed, the three-fold symmetry and weak-field ligand environment should promote a high-spin S = 5/2 ground state. However, given the nearly idealized C_3 symmetry displayed by **FeL^{OCH2O}** in the solid state, a maximally rhombic EPR spectrum would be surprising. Instead, we posit that this EPR signal is attributable to an impurity or decomposition product of **FeL^{OCH2O}**. Indeed, the g ≈ 4.3 signal originating from rhombic S = 5/2 species is very intense, and can dominate X-band EPR spectra even when present at very low concentrations.[28]

Chemical oxidation of **[FeL^{OMe}]$^-$** is conveniently performed using AgOTf (Figure 2). Following extraction of the crude reaction mixture with DMF, the solvento adduct **Fe(DMF)L^{OMe}** can be isolated via recrystallization as large cherry red crystals in good yields. Coordination of DMF at the axial coordination site leads to an increase to the *trans* Fe–N bond by nearly 0.1 Å compared to anionic **[FeL^{OMe}]$^-$** despite the increase in oxidation state at iron (Table S1). Performing the oxidation in CH_2Cl_2 without added DMF leads to intractable brown solids, emphasizing the ability of solvent coordination to stabilize the resulting neutral ferric complex. X-band EPR spectra of glassed MeCN solutions of **Fe(DMF)L^{OMe}** show features consistent with an axial spectrum (Figures 3 and S29), as anticipated for an iron(III) S = 5/2 spin system in a C_3-symmetric environment.[25,29–31] Additional features attributed to trace S = 5/2 and S = ½ impurities are also evident in the spectrum.

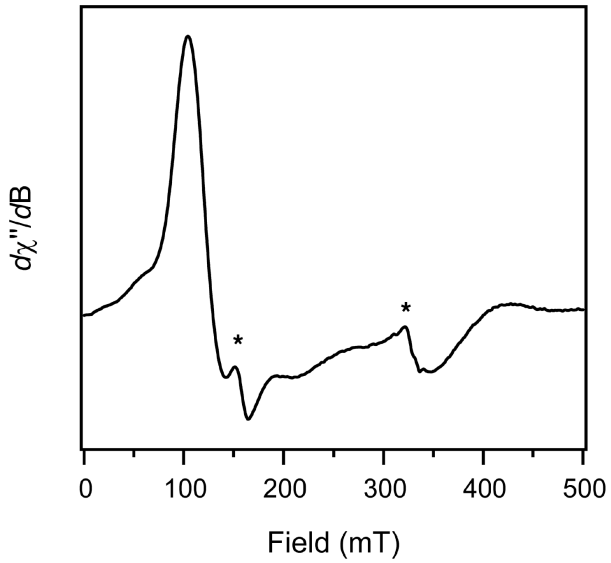

Figure 3. X-band EPR spectrum of a glassed MeCN solution of **Fe(DMF)L^{OMe}** at 10 K. The spectrum displays peaks at g_{eff} of 5.86 and 1.92 consistent with an axial zero-field splitting. Smaller features at $g_{eff} \approx 4.3$ and 2.0 (labeled with *) are attributed to rhombic $S = 5/2$ and isotropic $S = ½$ impurities, respectively. See Figure S29 for simulation details.

Both **FeL^{OCH2O}** and **Fe(DMF)L^{OMe}** give rise to a band in their electronic spectra with a λ_{max} near 400 nm (Figures S8–9). No such band is evident following oxidation of **[FeL^{OMe}]$^-$** in CH_2Cl_2 (Figure S10), suggesting that incipient four-coordinate **FeL^{OMe}** is too unstable in solution to be observed at ambient temperature. While **FeL^{OCH2O}** decays over the course of hours in CH_2Cl_2 at 23 ºC, DMF coordination imparts greatly improved stability to solutions of **Fe(DMF)L^{OMe}**, which undergo negligible decay over 5 h at 23 ºC (Figure S9).

Molecular dynamics simulations were carried out to interrogate the flexibility accessible to both the primary and secondary coordination spheres of the trigonal monopyramidal complexes **[FeL^{OMe}]$^-$**, **[FeL^{OCH2O}]$^-$** and **FeL^{OCH2O}**. In our simulations, special attention was paid to two geometric parameters, as they report on regions of space through which an exogenous reactant could conceivably access the unsaturated metal center. The first is the aperture width at the cavity rim (assessed for **[FeL^{OCH2O}]$^-$** and **FeL^{OCH2O}** only), which is approximated as the

mean distance between the *para* C–*H* atoms and incorporating the van der Waals radii of the H atoms (Figure S13). The second parameter is the equatorial N_{eq}–Fe–N_{eq} angles which, as they widen, expose a portion of the iron center to the exterior environment (Figure 4a). As seen in Figure S14 and the associated trajectory videos (see ESI), our simulations suggest that minimal changes to the aperture width as defined above are accessible to **FeL^{OCH2O}** or **[FeL^{OCH2O}]$^{-}$**. This result is in accord with the rigid nature of cavitands,[32,33] which are structurally analogous to the macrocycle comprising [L^{OCH2O}]$^{3-}$, and to the previously observed ability of this macrocycle to preclude acetonitrile binding to **[CoL^{OCH2O}]$^{-}$**.[16] However, simulations also indicate that a significant amount of flexibility is accessible in the equatorial plane of the metal coordination sphere, with N_{eq}–Fe–N_{eq} angles oscillating between approximately 105–135º for all three complexes (Figures 4b–c and S15). These results indicate that flexibility within the primary coordination sphere is minimally impacted by the presence of a rigid macrocycle in the secondary coordination sphere.

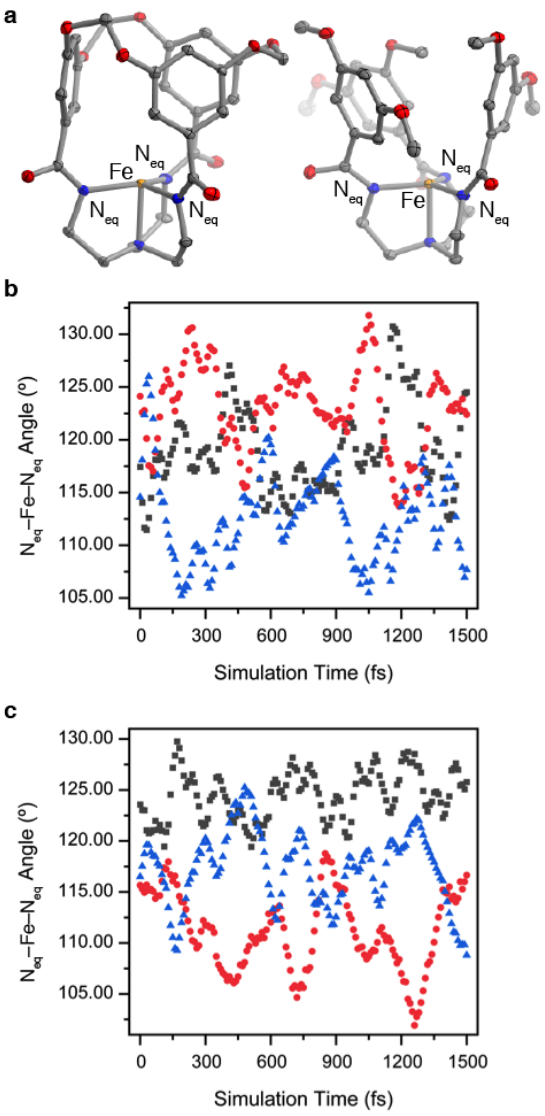

Figure 4. a) Depictions of the equatorial angles monitored during the course of MD simulations with complexes of the two tris(amidate)amine ligands. b) Equatorial N–Fe–N angles for **[FeL^{OCH2O}]$^{-}$**. c) Equatorial N–Fe–N angles for **[FeL^{OMe}]$^{-}$**. For the plots in (b) and (c), the colors arbitrarily denote the three possible N_{eq}–Fe–N_{eq} angles in each structure.

We note that Jahn-Teller distorted **[NiL^{OCH2O}]$^{-}$** showed equatorial N–Ni–N angles as ranging between 100–141° in the solid-state,[16] supporting the notion that angles of this magnitude can realistically occur within the [L^{OCH2O}]$^{3-}$ ligand framework. By transiently exposing some of the metal coordination sphere to the exterior environment, wagging motions in

the equatorial plane could ostensibly allow for coordination of an exogenous ligand to the metal without requiring passage through the macrocycle aperture (Figure 5, top). For instance, we hypothesize that transfer of an oxygen atom from iodosylbenzene to **[FeL^{OCH2O}]$^{-}$** to yield the previously reported ferryl oxo **[Fe(O)L^{OCH2O}]$^{-}$** exploits this pathway, as this O-atom transfer reagent is far too large to penetrate the macrocycle interior.[18] In contrast, an axial approach of exogenous ligands requires ingress via the 18-membered ring that forms the organic macrocycle (Figure 5, bottom). Axial approach of acetonitrile to trigonal monopyramidal [CoL^{OCH2O}]$^{-}$ was previously shown to be sterically impeded, attesting to the rigid and narrow void that is evident from our simulations.

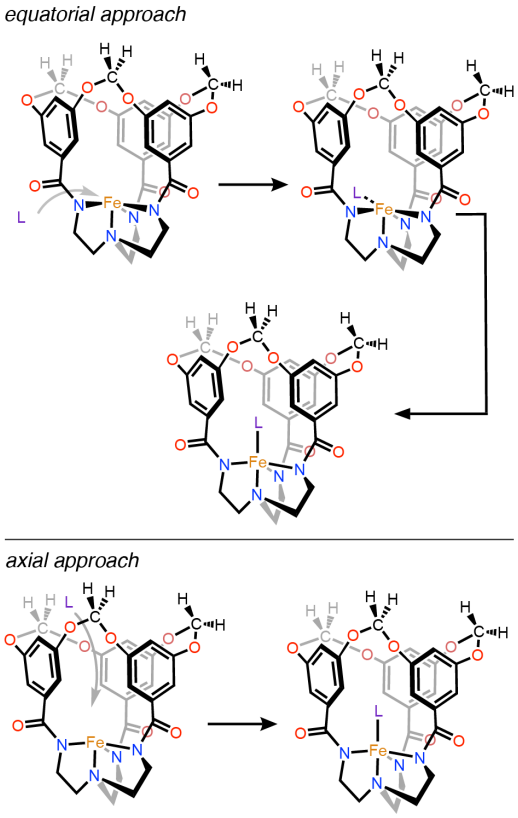

Figure 5. Top: Equatorial approach of small-profile ligands ("L") to **FeL^{OCH2O}** through the equatorial plane, hypothesized to occur via the N_{eq}–Fe–N_{eq} motions visualized using MD simulations. Bottom: Axial approach of exogenous ligands, which requires passage through the macrocycle aperture defined by the 18-membered ring.

Oxidation of **[FeL^{OCH2O}]**$^{-}$ and **[FeL^{OMe}]**$^{-}$ from iron(II) to iron(III) imparts enhanced Lewis acidity to the iron centers, facilitating the coordination of small X-type ligands at the axial coordination site.[18] We have synthesized the ferric fluoride **[K(Crypt)][Fe(F)L^{OCH2O}]** through addition of potassium fluoride and [2.2.2]cryptand to unpurified samples of **FeL^{OCH2O}**. Unlike four-coordinate **FeL^{OCH2O}**, the fluoride adduct can be synthesized in analytically pure form and displays greatly enhanced stability in solution. Reaction between **FeL^{OCH2O}** and F^{-} occurs rapidly as assessed by the color change from reddish brown to light yellow observed upon mixing. We hypothesize that initial binding of fluoride to iron occurs through the equatorial plane; although an axial "through-aperture" approach would force the charge-dense fluoride ion through the electron-rich arene-lined cavity, we cannot rule out such a pathway. Additionally, the corresponding fluoride complex **TBA[Fe(F)L^{OMe}]**$^{-}$ (TBA^{+} = tetra(*n*-butyl)ammonium) has been prepared from **Fe(DMF)L^{OMe}** via substitution of the DMF ligand using TBAF. Both anionic iron(III) fluoride complexes adopt trigonal bipyramidal coordination geometries with the fluoride ligand residing in the axial coordination site (Figures 6a–b and S35–36). Solution phase effective magnetic moment measurements are in accord with high-spin (S = 5/2) electronic ground states. Additionally, both species give rise to axial signals in their X-band EPR spectra (Figures 6c–d and S30–31). These compounds add to the small number of structurally characterized unsaturated ferric fluorides.[34–40]

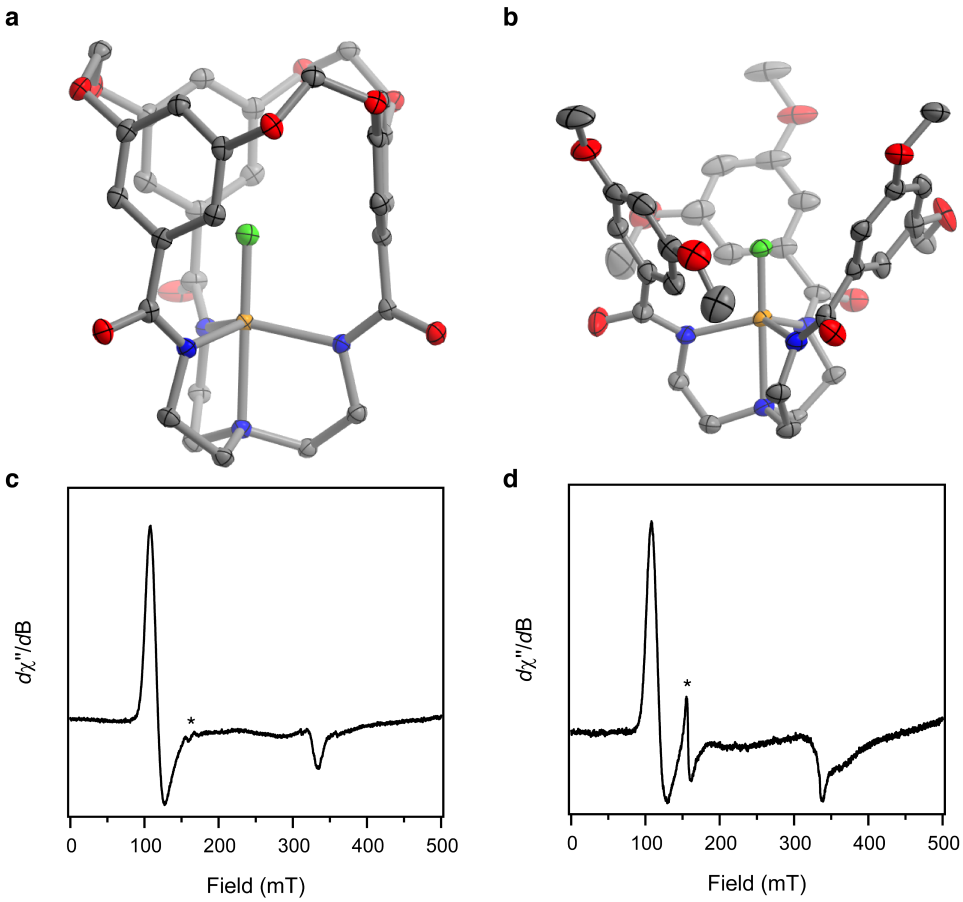

Figure 6. Solid state structures of (a) **[K(Crypt)][Fe(F)L^{OCH2O}]** and (b) **[TBA][Fe(F)L^{OMe}]**. Non-coordinating cations and hydrogen atoms have been omitted for clarity. Thermal ellipsoids are shown at the 50% probability level. X-band EPR spectra of (c) **[K(Crypt)][Fe(F)L^{OCH2O}]** and (d) **[TBA][Fe(F)L^{OMe}]** obtained in glassed CH_2Cl_2 solution at 10 K. Both spectra show a peak at g ≈ 4.3 (labeled with *) attributable to a trace S = 5/2 rhombic impurity. See Figures S30–31 for spectral simulation parameters.

Conclusion

In conclusion, oxidation of the anionic ferrous species **[FeL^{OCH2O}]$^{-}$** and **[FeL^{OMe}]$^{-}$** allows access to neutral trivalent complexes. While the resulting trigonal monopyramidal complexes of iron(III) display poor kinetic stability, the rigid macrocycle in the [L^{OCH2O}]$^{3-}$ framework permits isolation of this species, while solvent coordination imparts stability to the more flexible complex of [L^{OMe}]$^{3-}$. Both **FeL^{OCH2O}** and **Fe(DMF)L^{OMe}** can be used to generate five-coordinate

anionic complexes of trivalent iron as demonstrated through the syntheses of the corresponding fluoride complexes. Molecular dynamics simulations strongly suggest that equatorial distortions provide a plausible route for ligand coordination in **[FeL^{OCH2O}]^{n}** (n = –1, 0) that obviates penetration of the macrocycle aperture. Future studies will leverage these insights to understand and predict the outcome of intermolecular reactions involving complexes of the [L^{OCH2O}]$^{3-}$ ligand platform.

Corresponding Author

Brandon R. Barnett – *Department of Chemistry, University of Rochester, Rochester, New York 14627, United States;* https://orcid.org/0000-0002-3113-7347

Email: brandon.barnett@rochester.edu

Authors

Lucy S. X. Huffman – *Department of Chemistry, University of Rochester, Rochester, New York 14627, United States*; https://orcid.org/0000-0002-3890-246X

Anjana Seshadri‡ – *Department of Chemical Engineering, University of Rochester, Rochester, New York 14627, United States;* https://orcid.org/0009-0006-5957-6567

Christopher D. Hastings – *Department of Chemistry, University of Rochester, Rochester, New York 14627, United States*; https://orcid.org/0009-0000-2269-7601

William W. Brennessel – *Department of Chemistry, University of Rochester, Rochester, New York 14627, United States*; https://orcid.org/0009-0001-5461-1825

Ignacio Franco – *Department of Chemistry, University of Rochester, Rochester, New York 14627, United States; Department of Physics, University of Rochester, Rochester, New York 14627, United States;* https://orcid.org/0000-0002-0802-8185

Notes

The authors declare no competing financial interests.

‡Present address: Department of Materials Science and Engineering, Cornell University, Ithaca, NY, 14853

Acknowledgements

The work of L.S.X.H., C.D.H., and B.R.B. was supported by the National Science Foundation through a CAREER award to B.R.B. (CHE-2339280), as well as the American Chemical Society Petroleum Research Fund (66140-DNI3 to B.R.B.). The work of A.S. and I.F. was supported by the National Science Foundation (CHE-2416048 to I.F.). We thank Prof. Ellen M. Matson for the use of their electronic spectrometer, Adam Russell for assistance with the analysis of electronic spectroscopy data, and Dr. Bittu Chandra for assistance with EPR spectra. We also thank Profs. A. S. Borovik (UC Irvine) and Michael P. Hendrich (Carnegie Mellon University) for helpful discussions.

References

1 P. J. Chirik and K. Wieghardt, *Science*, 2010, **327**, 794–795.

2 M. L. Neidig, S. H. Carpenter, D. J. Curran, J. C. Demuth, V. E. Fleischauer, T. E. Iannuzzi, P. G. N. Neate, J. D. Sears and N. J. Wolford, *Acc. Chem. Res.*, 2019, **52**, 140–150.

3 M. Sono, M. P. Roach, E. D. Coulter and J. H. Dawson, *Chem. Rev.*, 1996, **96**, 2841–2887.

4 B. E. R. Snyder, P. Vanelderen, M. L. Bols, S. D. Hallaert, L. H. Böttger, L. Ungur, K. Pierloot, R. A. Schoonheydt, B. F. Sels and E. I. Solomon, *Nature*, 2016, **536**, 317–321.

5 A. D. N. Vaz, D. F. McGinnity and M. J. Coon, *Proc. Natl. Acad. Sci.*, 1998, **95**, 3555–3560.

6 J. Kaizer, E. J. Klinker, N. Y. Oh, J.-U. U. Rohde, W. J. Song, A. Stubna, J. Kim, E. Münck, W. Nam and L. Que, *J. Am. Chem. Soc.*, 2004, **126**, 472–473.

7 Y. Gao and J. M. Smith, *Acc. Chem. Res.*, 2023, **56**, 3392–3403.

8 M. Ghosh, K. K. Singh, C. Panda, A. Weitz, M. P. Hendrich, T. J. Collins, B. B. Dhar and S. Sen Gupta, *J. Am. Chem. Soc.*, 2014, **136**, 9524–9527.

9 B. Meunier, S. P. de Visser and S. Shaik, *Chem. Rev.*, 2004, **104**, 3947–3980.

10 S. A. Cook, E. A. Hill and A. S. Borovik, *Biochemistry*, 2015, **54**, 4167–4180.

11 M. W. Drover, *Chem. Soc. Rev.*, 2022, **51**, 1861–1880.

12 C. L. Ford, Y. J. Park, E. M. Matson, Z. Gordon and A. R. Fout, *Science*, 2016, **354**, 741–743.

13 C.-Y. Yeh, C. J. Chang and D. G. Nocera, *J. Am. Chem. Soc.*, 2001, **123**, 1513–1514.

14 D. Dhar, G. M. Yee and W. B. Tolman, *Inorg. Chem.*, 2018, **57**, 9794–9806.

15 R. Banerjee and J. D. Lipscomb, *Acc. Chem. Res.*, 2021, **54**, 2185–2195.

16 C. D. Hastings, L. S. X. Huffman, C. K. Tiwari, J. G. Betancourth, W. W. Brennessel and B. R. Barnett, *Inorg. Chem.*, 2023, **62**, 11920–11931.

17 M. E. Zapesochny, C. D. Hastings, W. W. Brennessel, B. R. Barnett, M. E. Zapesochny, C. D. Hastings, W. William, M. E. Zapesochny, C. D. Hastings, W. W. Brennessel and B.

R. Barnett, *J. Coord. Chem.*, 2025, Ahead of Print. DOI: 10.1080/00958972.2025.2495055.

18 C. D. Hastings, L. S. X. Huffman, W. W. Brennessel and B. R. Barnett, *J. Am. Chem. Soc.*, 2025, **147**, 14031–14035.

19 C. C. Cummins, J. Lee, R. R. Schrock and W. D. Davis, *Angew. Chem. Int. Ed.*, 1992, **31**, 1501–1503.

20 C. C. Cummins and R. R. Schrock, *Inorg. Chem.*, 1994, **33**, 395–396.

21 C. Souilah, S. A. V Jannuzzi, D. Demirbas, S. Ivlev, M. Swart, S. DeBeer and A. Casitas, *Angew. Chemie Int. Ed.*, 2022, **61**, e202201699.

22 G. E. Alliger, P. Müller, L. H. Do, C. C. Cummins and D. G. Nocera, *Inorg. Chem.*, 2011, **50**, 4107–4115.

23 J. Chen and L. K. Woo, *J. Organomet. Chem.*, 2000, **601**, 57–68.

24 N. S. Sickerman, S. M. Peterson, J. W. Ziller and A. S. Borovik, *Chem. Commun.*, 2014, **50**, 2515–2517.

25 C. Sun, V. F. Oswald, E. A. Hill, J. W. Ziller and A. S. Borovik, *Dalton Trans.*, 2021, **50**, 11197–11205.

26 L. Yang, D. R. Powell and R. P. Houser, *Dalton Trans.*, 2007, 955–964.

27 N. Elgrishi, K. J. Rountree, B. D. McCarthy, E. S. Rountree, T. T. Eisenhart and J. L. Dempsey, *J. Chem. Educ.*, 2018, **95**, 197–206.

28 J. Telser, "EPR Interactions – Zero-field Splittings", in EPR Spectroscopy: Fundamentals and Methods, eds. D. Goldfarb and S. Stoll, John Wiley & Sons, Hoboken, NJ, USA, 2018, ch. 3, pp. 29–62.

29 D. C. Bradley, R. G. Copperthwaite, S. A. Cotton, K. D. Sales and J. F. Gibson, *J. Chem.*

Soc. Dalton Trans., 1973, 191–194.

30 W. V. Sweeney, D. Coucouvanis and R. E. Coffman, *J. Chem. Phys.*, 1973, **59**, 369–379.

31 Note that we cannot rule out substitution of the DMF ligand for an equivalent of MeCN under these conditions, as trigonal bipyramidal adducts with either solvent would be expected to give rise to similar spectral features.

32 J. R. Moran, S. Karbach and D. J. Cram, *J. Am. Chem. Soc.*, 1982, **104**, 5826–5828.

33 C. M. Kane, O. Ugono, L. J. Barbour, K. Travis Holman, C. M. Kane, O. Ugono, L. J. Barbour and K. T. Holman, *Chem. Mater.*, 2015, **27**, 7337–7354.

34 D. Sakow, D. Baabe, B. Böker, O. Burghaus, M. Funk, C. Kleeberg, D. Menzel, C. Pietzonka and M. Bröring, *Chem. Eur. J.*, 2014, **20**, 2913–2924.

35 Q. Zhang, L. Xiang and L. Deng, *Organometallics*, 2012, **31**, 4537–4543.

36 S. C. Lee and R. H. Holm, *Inorg. Chem.*, 1993, **32**, 4745–4753.

37 K. Anzai, K. Hatano, Y. J. Lee and W. R. Scheidt, *Inorg. Chem.*, 1981, **20**, 2337–2339.

38 S. Kuppuswamy, T. M. Powers, B. M. Johnson, C. K. Brozek, J. P. Krogman, M. W. Bezpalko, L. A. Berben, J. M. Keith, B. M. Foxman and C. M. Thomas, *Inorg. Chem.*, 2014, **53**, 5429–5437.

39 G. De Ruiter, N. B. Thompson, M. K. Takase and T. Agapie, *J. Am. Chem. Soc.*, 2016, **138**, 1486–1489.

40 G. W. Farley, M. A. Siegler and D. P. Goldberg, *Inorg. Chem.*, 2021, **60**, 17288–17302.

All data supporting this research are included in the main article and/or the ESI, except for the crystallographic information files (CIFs), which are available from the Cambridge Crystallographic Data Centre free of charge (accession numbers 2422256–2422260).